Title: Straightforward FRAP for quantitative diffusion measurements with a laser scanning microscope

Authors: H. Deschout, J. Hagman, S. Fransson, J. Jonasson, M. Rudemo, N. Lorén, K. Braeckmans

In: Optics Express, 18(22), 2286-22905 (2010)

Straightforward FRAP for quantitative diffusion measurements with a laser scanning microscope

Hendrik Deschout,[1] Joel Hagman,[2] Sophia Fransson,[2] Jenny Jonasson,[3] Mats Rudemo,[3] Niklas Lorén,[2] and Kevin Braeckmans[1,*]

[1]*Biophotonic Imaging Group, Lab. General Biochemistry and Physical Pharmacy, Ghent University, Harelbekestraat 72, B-9000 Gent, Belgium*
[2]*Structure and Material Design, SIK, The Swedish Institute for Food and Biotechnology, Box 5401, SE-402 29 Göteborg, Sweden*
[3]*Mathematical Sciences, Chalmers University of Technology and Gothenburg University, SE-41296 Göteborg, Sweden*
[*]*Kevin.Braeckmans@UGent.be*

Abstract: Confocal or multi-photon laser scanning microscopes are convenient tools to perform FRAP diffusion measurements. Despite its popularity, accurate FRAP remains often challenging since current methods are either limited to relatively large bleach regions or can be complicated for non-specialists. In order to bring reliable quantitative FRAP measurements to the broad community of laser scanning microscopy users, here we have revised FRAP theory and present a new pixelbased FRAP method relying on the photobleaching of rectangular regions of any size and aspect ratio. The method allows for fast and straightforward quantitative diffusion measurements due to a closed–form expression for the recovery process utilising all available spatial and temporal data. After a detailed validation, its versatility is demonstrated by diffusion studies in heterogeneous biopolymer mixtures.

OCIS codes: (170.0170) Medical optics and biotechnology; (170.1790) Confocal microscopy; (180.0180) Microscopy; (180.2520) Fluorescence microscopy.

References and links

1. M. Edidin, "Translational diffusion of membrane proteins," in *The Structure of Biological Membranes*, P. Yeagle, ed., (CRC Press, Boca Raton, 1992), pp. 539-572.
2. A. Ishihara and K. Jacobson, "A Closer Look at How Membrane-Proteins Move," Biophysical Journal **65**, 1754-1755 (1993).
3. F. Umenishi, J. M. Verbavatz, and A. S. Verkman, "cAMP regulated membrane diffusion of a green fluorescent protein-aquaporin 2 chimera," Biophysical Journal **78**, 1024-1035 (2000).
4. F. Alvarez-Mancenido, K. Braeckmans, S. C. De Smedt, J. Demeester, M. Landin, and R. Martinez-Pacheco, "Characterization of diffusion of macromolecules in konjac glucomannan solutions and gels by fluorescence recovery after photobleaching technique," International Journal of Pharmaceutics **316**, 37-46 (2006).
5. M. D. Burke, J. O. Park, M. Srinivasarao, and S. A. Khan, "Diffusion of macromolecules in polymer solutions and gels: A laser scanning confocal microscopy study," Macromolecules **33**, 7500-7507 (2000).
6. Censi R., Vermonden T., van Steenbergen M.J., Deschout H., Braeckmans K., De Smedt S.C., van Nostrum C.F., di Martino P., and Hennink W.E., "Photopolymerized thermosensitive hydrogels for tailorable diffusion-controlled protein delivery," Journal of Controlled Release **140**, 230-236 (2009).
7. S. C. DeSmedt, T. K. L. Meyvis, J. Demeester, P. VanOostveldt, J. C. G. Blonk, and W. E. Hennink, "Diffusion of macromolecules in dextran methacrylate solutions and gels as studied by confocal scanning laser microscopy," Macromolecules **30**, 4863-4870 (1997).
8. F. van de Manakker, K. Braeckmans, N. el Morabit, S. C. De Smedt, C. F. van Nostrum, and W. E. Hennink, "Protein-Release Behavior of Self-Assembled PEG-beta-Cyclodextrin/PEG-Cholesterol Hydrogels," Advanced Functional Materials **19**, 2992-3001 (2009).
9. S. R. Van Tomme, B. G. De Geest, K. Braeckmans, S. C. De Smedt, F. Siepmann, J. Siepmann, van Nostrum C.F., and W. E. Hennink, "Mobility of model proteins in hydrogels composed of oppositely charged

dextran microspheres studied by protein release and fluorescence after photobleaching," Journal of Controlled Release **110**, 67-78 (2005).

10. J. Braga, J. M. P. Desterro, and M. Carmo-Fonseca, "Intracellular macromolecular mobility measured by fluorescence recovery after photobleaching with confocal laser scanning microscopes," Molecular Biology of the Cell **15**, 4749-4760 (2004).
11. O. Seksek, J. Biwersi, and A. S. Verkman, "Translational diffusion of macromolecule-sized solutes in cytoplasm and nucleus," Journal of Cell Biology **138**, 131-142 (1997).
12. A. S. Verkman, "Diffusion in cells measured by fluorescence recovery after photobleaching," Biophotonics, Pt A **360**, 635-648 (2003).
13. D. Axelrod, D. E. Koppel, J. Schlessinger, E. Elson, and W. W. Webb, "Mobility Measurement by Analysis of Fluorescence Photobleaching Recovery Kinetics," Biophysical Journal **16**, 1055-1069 (1976).
14. K. Braeckmans, B. G. Stubbe, K. Remaut, J. Demeester, and S. C. De Smedt, "Anomalous photobleaching in fluorescence recovery after photobleaching measurements due to excitation saturation- a case study for fluorescein," Journal of Biomedical Optics **11**, (2006).
15. K. Braeckmans, K. Remaut, R. E. Vandenbroucke, B. Lucas, S. C. De Smedt, and J. Demeester, "Line FRAP with the confocal laser scanning microscope for diffusion measurements in small regions of 3-D samples," Biophysical Journal **92**, 2172-2183 (2007).
16. D. Mazza, K. Braeckmans, F. Cella, I. Testa, D. Vercauteren, J. Demeester, S. S. De Smedt, and A. Diaspro, "A new FRAP/FRAPa method for three-dimensional diffusion measurements based on multiphoton excitation microscopy," Biophysical Journal **95**, 3457-3469 (2008).
17. K. Braeckmans, L. Peeters, N. N. Sanders, S. C. De Smedt, and J. Demeester, "Three-dimensional fluorescence recovery after photobleaching with the confocal scanning laser microscope," Biophysical Journal **85**, 2240-2252 (2003).
18. D. A. Berk, F. Yuan, M. Leunig, and R. K. Jain, "Fluorescence Photobleaching with Spatial Fourier-Analysis - Measurement of Diffusion in Light-Scattering Media," Biophysical Journal **65**, 2428-2436 (1993).
19. P. Jonsson, M. P. Jonsson, J. O. Tegenfeldt, and F. Hook, "A Method Improving the Accuracy of Fluorescence Recovery after Photobleaching Analysis," Biophysical Journal **95**, 5334-5348 (2008).
20. T. T. Tsay and K. A. Jacobson, "Spatial Fourier-Analysis of Video Photobleaching Measurements - Principles and Optimization," Biophysical Journal **60**, 360-368 (1991).
21. J. K. Jonasson, N. Loren, P. Olofsson, M. Nyden, and M. Rudemo, "A pixel-based likelihood framework for analysis of fluorescence recovery after photobleaching data," Journal of Microscopy-Oxford **232**, 260-269 (2008).
22. J. K. Jonasson, J. Hagman, N. Loren, D. Bernin, M. Nyden, and M. Rudemo, "Pixel-based analysis of FRAP data with a general initial bleaching profile," Journal of Microscopy-Oxford **239**, 142-153 (2010).
23. A. Tannert, S. Tannert, S. Burgold, and M. Schaefer, "Convolution-based one and two component FRAP analysis: theory and application," European Biophysics Journal with Biophysics Letters **38**, 649-661 (2009).
24. P. Wedekind, U. Kubitscheck, and R. Peters, "Scanning Microphotolysis - A New Photobleaching Technique Based on Fast Intensity Modulation of A Scanned Laser-Beam and Confocal Imaging," Journal of Microscopy-Oxford **176**, 23-33 (1994).
25. P. Wedekind, U. Kubitscheck, O. Heinrich, and R. Peters, "Line-scanning microphotolysis for diffraction-limited measurements of lateral diffusion," Biophysical Journal **71**, 1621-1632 (1996).
26. E. B. Brown, E. S. Wu, W. Zipfel, and W. W. Webb, "Measurement of molecular diffusion in solution by multiphoton fluorescence photobleaching recovery," Biophysical Journal **77**, 2837-2849 (1999).
27. J. Crank, *The Mathematics of Diffusion*, (Clarendon Press, Oxford, 1975).
28. J. C. G. Blonk, A. Don, H. Vanaalst, and J. J. Birmingham, "Fluorescence Photobleaching Recovery in the Confocal Scanning Light-Microscope," Journal of Microscopy-Oxford **169**, 363-374 (1993).
29. Y. Pawitan, *In All Likelihood*, (Clarendon Press, Oxford, 2001).
30. W. H. Press, S. A. Teukolsky, W. T. Vetterling, and B. P. Flannery, "Confidence Limits on Estimated Model Parameters," in *Numerical Recipes in C*, (Cambridge University Press, Cambridge, 1992).
31. M. Kang, C. A. Day, K. Drake, A. K. Kenworthy, and E. DiBenedetto, "A Generalization of Theory for Two-Dimensional Fluorescence Recovery after Photobleaching Applicable to Confocal Laser Scanning Microscopes," Biophysical Journal **97**, 1501-1511 (2009).
32. S. Fransson, N. Loren, A. Altskar, and A. M. Hermansson, "Effect of Confinement and Kinetics on the Morphology of Phase Separating Gelatin-Maltodextrin Droplets," Biomacromolecules **10**, 1446-1453 (2009).
33. N. Loren, A. Altskar, and A. M. Hermansson, "Structure evolution during gelation at later stages of spinodal decomposition in gelatin/maltodextrin mixtures," Macromolecules **34**, 8117-8128 (2001).
34. N. Loren and A. M. Hermansson, "Phase separation and gel formation in kinetically trapped gelatin/maltodextrin gels," International Journal of Biological Macromolecules **27**, 249-262 (2000).

35. N. Loren and A. M. Hermansson, "Structure evolution during phase separation and gelation of biopolymer mixtures," in *Food Colloids - Biopolymers and Materials*, Dickinson E. and Van Vliet T., eds., (The Royal Society of Chemistry, Cambridge, 2003), pp. 298-308.

1. Introduction

Molecular transport is essential for the functionality of cells and for the properties of many industrial products such as pharmaceuticals, pharmaceutical devices, foods, cosmetics etc. Different methods based on fluorescence microscopy exist to characterize the local mobility of molecules in terms of a diffusion coefficient. One of them is fluorescence recovery after photobleaching (FRAP), which is most useful for studying diffusion in the range of 0.1 to 100 $\mu m^2/s$ on a micrometer scale. FRAP diffusion measurements are based on creating a concentration gradient through local photobleaching of the fluorescently labelled molecules, which is the photochemical process through which a fluorescent molecule loses its fluorescence properties after being excited by an incoming photon. By illuminating a certain area in the microscope sample with high-intensity excitation light, the fluorescent molecules within that area can photobleach, leading to a local reduction in fluorescence intensity. Exchange via diffusion of these photobleached molecules with intact fluorescent molecules outside the illuminated area leads to a gradual recovery of the fluorescence inside that area. The rate of fluorescence recovery is proportional to the rate of diffusion of the fluorescently labelled molecules. Using a suitable FRAP model, analysis of the fluorescence recovery can yield the physical quantities describing the local diffusion in the sample, such as the diffusion coefficient in case of free diffusion. FRAP has become a popular technique to study the diffusion of molecules in a variety of systems like cell membranes [1-3], polymer gel systems [4-9] and living cells [10-12].

The first FRAP methods were developed in the 1970s, using fluorescence microscopes with non-scanning lasers as light sources and photo-multiplier tubes as detectors [13]. The photobleached area was determined by the intensity distribution of the focused laser beam which had either a Gaussian or a uniform circular profile. As the fluorescence recovery was monitored by the same (attenuated) laser beam, only temporal information was available of the fluorescence recovery (i.e. spot photobleaching measurements). To include spatial information as well, video cameras were used during the 1980s, allowing visualisation of the fluorescence recovery inside and outside the photobleached region. During this period, also the confocal laser scanning microscope (CLSM) became available, opening up new possibilities for more flexible FRAP experiments.

By means of the scanning laser beam of a CLSM it is possible to define a photobleaching area of any size and shape, resulting in a large range of detectable diffusion coefficients. Since confocal microscopy is an imaging technique, both spatial and temporal information are in principle available from the recovery images. However, due to the mathematical complexity of the problem, quantitative interpretation of FRAP data to date remains mostly limited to temporal analysis of the average fluorescence in the photobleached area. When spatial information is not taken into account, a prerequisite for accurate results is the exact knowledge of the initial concentration of bleached molecules after photobleaching. However, because of non-linear saturation effects during the highly intense photobleaching phase that depend on the photon flux, the type of fluorophore and the local chemical environment, it is very difficult to estimate or calibrate the initial bleaching profile exactly [14-16]. While these non-linear effects can be neglected when using large photobleaching areas [17], they have a substantial effect when using small areas close to the resolution of the microscope [15,16].

The necessity of *a priori* knowledge of the exact initial bleaching profile can be circumvented by taking into account the spatial information of the recovery images. Inventive FRAP models have been proposed along this line that make use of mathematical transformations, such as the Fourier transform or Hankel transform [18-20]. However, the

methods published so far do not take the microscope's imaging point-spread function into account so that deviations could arise for very small regions. Moreover, these methods have not been extended to 3-D diffusion for e.g. 2-photon FRAP measurements [16]. A pixelbased maximum likelihood framework was reported, assuming that the initial bleaching profile can be approximated by a Gaussian distribution [21]. To alleviate the latter restriction, recently a numerical method has been introduced [22], where the maximum likelihood framework is extended to a general initial profile only assuming that the profile is a non-decreasing function of the distance to the bleaching centre. While this method is accurate for all types of initial profiles studied, similar to other numerical approaches [23-25], it generally requires special programming expertise, while data analysis can take hours on modern computers. Therefore, there remains the need for quantitative but straightforward and fast FRAP methods that take the full spatial and temporal information into account without posing any restrictions on the size of the bleaching area.

In order to bring highly reliable quantitative FRAP measurements to the broad community of laser scanning microscopy users, here we present a new and versatile FRAP model that describes the full temporal and spatial diffusion process after photobleaching by a scanning laser beam of an arbitrary rectangular area (rFRAP). A rectangular area was chosen instead of the more typical circular region because this enabled us to find a closed-form expression for the recovery process, thus allowing for fast and straightforward analysis of the recovery images. Moreover, by taking the microscope's effective photobleaching and imaging resolution into account, the rectangle can have any size and aspect ratio, thus providing for maximum flexibility. The new pixelbased FRAP model effectively utilises all information in the image set to estimate the diffusion rate. First we give an outline of the mathematical derivation leading to the general 3-D multi-photon FRAP expression, followed by a discussion on the practical 2-D limit for single photon CLSM experiments. We present a detailed experimental validation of the method where we demonstrate that the method is valid for any size and aspect ratio of the rectangle. Furthermore we compare two ways of analyzing the recovery images, either by a straightforward least squares analysis or by a robust maximum likelihood framework. Finally we demonstrate the usefulness and versatility of the method on a mixed biopolymer system of gelatin and maltodextrin which is of relevance to the food and pharmaceutical industry.

2. Theory

2.1 Derivation of the general rFRAP expression

Consider a sample with a uniform concentration C_0 of fluorescent molecules. Let $I_b^n(x,y,z,t)$ be the *n*-photon illumination intensity distribution of the laser scanning microscope (LSM) with a temporal average intensity of the (pulsed) laser beam $\left\langle I_b^n(x,y,z,t)\right\rangle$. Assuming first order photobleaching kinetics and a short photobleaching time to avoid significant diffusion during bleaching, the fluorophore concentration C_b after *n*-photon photobleaching of a 2-D geometry $B(x,y)$ with a scanning beam can be calculated from [16]:

$$C_b(x,y,z) = C_0 e^{-\frac{\sigma_n q_n}{n v \Delta y} K(x,y,z)}, \qquad (1.1)$$

where σ_n is the *n*-photon absorption cross-section and q_n the quantum efficiency for *n*-photon photobleaching. v is the scanning speed of the laser beam and Δy the distance between adjacent scanning lines. The effective bleaching intensity distribution $K(x,y,z)$ is calculated

from the convolution product of the geometry $B(x,y)$ and the time-average bleaching intensity distribution:

$$K(x,y,z)=\int_{-\infty}^{+\infty}\int_{-\infty}^{+\infty}B(x',y')\left\langle I_b^n(x-x',y-y',z,t)\right\rangle \mathrm{d}x'\mathrm{d}y'. \tag{1.2}$$

Here we assume a rectangular photobleaching area as illustrated in Fig. 1:

$$B(x,y)=\begin{cases}1, & -\frac{l_x}{2}\le x\le+\frac{l_x}{2} \text{ and } -\frac{l_y}{2}\le y\le+\frac{l_y}{2}\\ 0, & \text{elsewhere}\end{cases} \tag{1.3}$$

and a Gaussian photobleaching intensity distribution [16,26]:

$$\left\langle I_b^n(x,y,z,t)\right\rangle=\left\langle I_b^n(0,0,0,t)\right\rangle e^{-2n\left(\frac{x^2+y^2}{r_{b,0}^2}+\frac{z^2}{z_{b,0}^2}\right)}, \tag{1.4}$$

where $r_{b,0}$ is the lateral and $z_{b,0}$ is the axial effective resolution for single photon photobleaching. $\left\langle I_b^n(0,0,0,t)\right\rangle$ is the temporal average intensity of the (pulsed) laser beam at the origin for *n*-photon photobleaching. Inserting Eq. (1.3) and (1.4) into Eq. (1.2) results in:

$$K(x,y,z)=\left\langle I_b^n(0,0,0,t)\right\rangle e^{-\frac{2n}{z_{b,0}^2}z^2}\int_{-\frac{l_x}{2}}^{+\frac{l_x}{2}}e^{-\frac{2n}{r_{b,0}^2}(x-x')^2}\mathrm{d}x'\int_{-\frac{l_y}{2}}^{+\frac{l_y}{2}}e^{-\frac{2n}{r_{b,0}^2}(y-y')^2}\mathrm{d}y'. \tag{1.5}$$

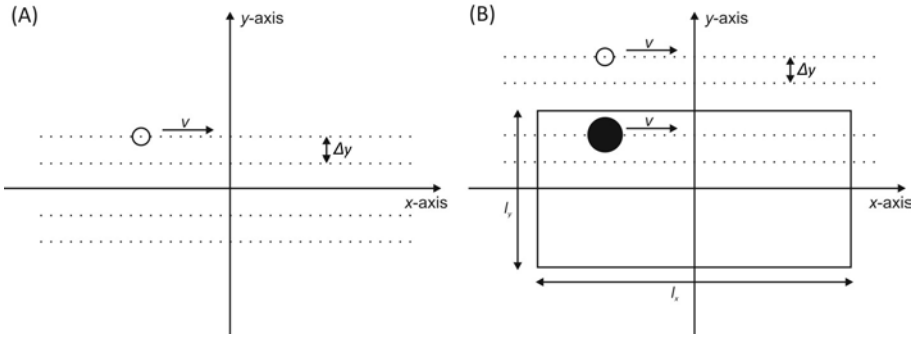

Fig. 1 : An illustration of the use of a confocal laser scanning microscope in performing a FRAP measurement. The scanning speed is *v* and the distance between the consecutive scanning lines is Δy. (A) Images are acquired by scanning the imaging point spread function (open circle) across the focal plane. (B) By increasing the laser intensity within the indicated rectangle, a rectangular area can be photobleached.

Since it is our aim to finally come to a closed-form expression, we further assume a limited amount of photobleaching such that the exponential photobleaching process from Eq. (1.1) can be approximated by a linear process (first order of the Taylor expansion):

$$C_b(x,y,z)=C_0-C_0\frac{\sigma_n q_n}{nv\Delta y}K(x,y,z). \tag{1.6}$$

We will show experimentally that this assumption in practice does not impose a big limitation. Furthermore, we will demonstrate that in practice diffusion during photobleaching in fact can be accounted for by the rectangle FRAP method, despite the fact that this is formally neglected at this point in the derivation. To model the fluorescence recovery after photobleaching of the rectangle, Fick's second law has to be solved for the initial condition in Eq. (1.6). Inserting Eq. (1.6) into the integral form of Fick's second law gives the concentration C of the fluorophores as a function of time and space after photobleaching [27]:

$$C(x,y,z,t) = \frac{1}{(4\pi Dt)^{\frac{3}{2}}} \int_{-\infty}^{+\infty}\int_{-\infty}^{+\infty}\int_{-\infty}^{+\infty} C_b(x-x', y-y', z-z') e^{-\frac{1}{4Dt}\left(x'^2+y'^2+z'^2\right)} \mathrm{d}x'\mathrm{d}y'\mathrm{d}z'. \quad (1.7)$$

Eq. (1.7). can be rewritten using Eq. (1.5), finally leading to:

$$\frac{C(x,y,z,t)}{C_0} = 1 - \frac{\sigma_n q_n}{nv\Delta y}\left\langle I_b^n(0,0,0,t)\right\rangle z_{b,0} r_{b,0}^2 \sqrt{\frac{1}{z_{b,0}^2+8nDt}\,\frac{1}{r_{b,0}^2+8nDt}} \times e^{-\frac{2n}{z_{b,0}^2+8nDt}z^2} \int_{-\frac{l_x}{2}}^{+\frac{l_x}{2}} e^{-\frac{2n}{r_{b,0}^2+8nDt}(x-x')^2}\mathrm{d}x' \int_{-\frac{l_y}{2}}^{+\frac{l_y}{2}} e^{-\frac{2n}{r_{b,0}^2+8nDt}(y-y')^2}\mathrm{d}y', \quad (1.8)$$

where D is the isotropic diffusion coefficient of the diffusing species. If the fluorescence recovery is imaged by m-photon microscopy, the observed fluorescence can be calculated from the convolution product of the real concentration according to Eq. (1.8) and the overall microscope's imaging point spread function $\left\langle I_d^m(x,y,z,t)\right\rangle$:

$$F(x,y,z,t) = q\int_{-\infty}^{+\infty}\int_{-\infty}^{+\infty}\int_{-\infty}^{+\infty}\left\langle I_d^m(x,y,z)\right\rangle C(x-x', y-y', z-z', t)\mathrm{d}x'\mathrm{d}y'\mathrm{d}z', \quad (1.9)$$

The imaging point spread function $\left\langle I_d^m(x,y,z,t)\right\rangle$ can be modelled as a 3-D Gaussian function:

$$\left\langle I_d^m(x,y,z,t)\right\rangle = \left\langle I_d^m(0,0,0,t)\right\rangle e^{-2m\left(\frac{x^2+y^2}{r_{d,0}^2}+\frac{z^2}{z_{d,0}^2}\right)}, \quad (1.10)$$

where $r_{d,0}$ is the lateral and $z_{d,0}$ is the axial resolution for single photon imaging. Note that we allow the resolution (radial and axial) of the imaging point spread function to be different from the bleaching intensity distribution in Eq. (1.4) since it was previously shown that saturation effects can increase the effective resolution of the bleaching intensity distribution [14-16]. First, define the following parameters as:

$$r_{m,n}^2 = \frac{\frac{r_{d,0}^2}{m}+\frac{r_{b,0}^2}{n}}{2},\ z_{m,n}^2 = \frac{\frac{z_{d,0}^2}{m}+\frac{z_{b,0}^2}{n}}{2},\ K_0 = \frac{\pi}{2}\frac{\sigma_n q_n}{nv\Delta y}\left\langle I_b^n(0,0,0,t)\right\rangle\left(\frac{r_{b,0}}{n}\right)^2. \quad (1.11)$$

Substituting Eq. (1.10) in (1.9) subsequently leads to:

$$\frac{F(x,y,z,t)}{F_0} = 1 - \frac{K_0}{4}\frac{z_{b,0}}{\sqrt{2n}}\frac{1}{\sqrt{z_{m,n}^2+4Dt}}e^{-\frac{1}{z_{m,n}^2+4Dt}z^2} \times\left[\operatorname{erf}\left(\frac{x+\frac{l_x}{2}}{\sqrt{r_{m,n}^2+4Dt}}\sqrt{}\right)-\operatorname{erf}\left(\frac{x-\frac{l_x}{2}}{\sqrt{r_{m,n}^2+4Dt}}\sqrt{}\right)\right] \times\left[\operatorname{erf}\left(\frac{y+\frac{l_y}{2}}{\sqrt{r_{m,n}^2+4Dt}}\sqrt{}\right)-\operatorname{erf}\left(\frac{y-\frac{l_y}{2}}{\sqrt{r_{m,n}^2+4Dt}}\sqrt{}\right)\right], \tag{1.12}$$

which describes the three-dimensional fluorescence recovery at a time t after photobleaching. Excitation is assumed to be an m- and n-photon process for imaging and bleaching, respectively, and the bleached area is a rectangle centred in the origin with width l_x and height l_y (see Fig. 1). Eq. (1.12) contains the error function, which is defined as $\operatorname{erf}(z) = \frac{2}{\sqrt{\pi}}\int_0^z e^{-x^2}\mathrm{d}x$.

2.2 Single photon rFRAP

It is useful to consider the case m=n=1 (we denote $r_{1,1}^2$ as r^2 in Eq. (1.11)) which corresponds to FRAP experiments performed on a regular (single photon) CLSM. However, in that case the above formula is incorrect as far as the axial diffusion is concerned (z-direction). This is because the single photon illumination profile has a conical shape which is not taken into account by Eq. (1.4) and this will lead to a discrepancy between the theory and the actual experiment. Therefore, when performing FRAP experiments on a regular (single photon) CLSM, diffusion along the optical axis should be avoided so that 2-D diffusion can be assumed. This is e.g. the case when the diffusion is restricted to a plane, such as for membrane transport. In a 3-D extended sample, a 2-D situation can be mimicked by using a low numerical aperture lens which produces a cylindrical illumination profile instead of a conical one [15,17,28]. In that case, there will be substantial photobleaching above and below the focal plane, thus avoiding net diffusion along the optical axis. The single photon 2-D rFRAP model can be derived from Eq. (1.12) by letting $z_{b,0}$ approach infinity, and setting m=n=1 and z=0 (observation in focal plane):

$$\frac{F(x,y,t)}{F_0} = 1 - \frac{K_0}{4}\left[\operatorname{erf}\left(\frac{x+\frac{l_x}{2}}{\sqrt{r^2+4Dt}}\right)-\operatorname{erf}\left(\frac{x-\frac{l_x}{2}}{\sqrt{r^2+4Dt}}\right)\right] \times\left[\operatorname{erf}\left(\frac{y+\frac{l_y}{2}}{\sqrt{r^2+4Dt}}\right)-\operatorname{erf}\left(\frac{y-\frac{l_y}{2}}{\sqrt{r^2+4Dt}}\right)\right]. \tag{1.13}$$

Note that the percentage of photobleaching P at the centre of the rectangle, follows immediately from $F(0,0,0)$:

$$P = 100 \times \left(1 - \frac{F(0,0,0)}{F_0}\right) = 100 \times \left(1 - K_0 \operatorname{erf}\left(\frac{l_x}{2r}\right) \operatorname{erf}\left(\frac{l_y}{2r}\right)\right). \qquad (1.14)$$

One special case is when the combination of a mobile and immobile fraction is assumed. Let k be the fraction of mobile molecules, the fluorescence $F_k(x,y,t)$ is then given by [15]:

$$F_k(x,y,t) = F(x,y,0) + k\left[F(x,y,t) - F(x,y,0)\right]. \qquad (1.15)$$

where $F(x,y,t)$ is defined by Eq. (1.13). All experiments presented in this work were analyzed using Eq. (1.13) and (1.15).

2.3 Parameter estimation by maximum likelihood and least squares fitting

As is illustrated in Fig. 2A, a CLSM FRAP experiment results in a time lapse movie consisting of one or more pre-bleach images, the photobleaching image (depending on the instrument) and the recovery images. After normalization to the initial fluorescence and optional correction for photobleaching during imaging, Eq. (1.13) or (1.15) can be fitted to the entire set of pixel values from the recovery images. Since all available data is used, this method achieves maximum precision and also allows to include the resolution parameter r^2 as a free fitting parameter. In this way calibration of the photobleaching resolution $r_{b,0}$ can be avoided [15]. We have evaluated two different fitting procedures, one based on classic least squares analysis and another one on a maximum likelihood framework.

Maximum likelihood is an efficient statistical method for estimating parameters of a model and which also gives standard errors of the estimated parameters [29]. To use it in this context, a probabilistic description of the noise is needed. Let $p(x,y,t)$ denote the pixel value at a pixel with coordinates (x,y) at time t. The pixel value or intensity is assumed to be linearly proportional to the number of photons $N(x,y,t)$ observed at that pixel, which we write as $p(x,y,t) = \beta N(x,y,t)$. The expectation of $p(x,y,t)$ is given by $F(x,y,t)$ from Eq. (1.13). Furthermore, we assume that $N(x,y,t)$ is Poisson distributed with expectation $F(x,y,t)/\beta$. The Poisson distribution is approximated by a normal distribution with expectation and variance $F(x,y,t)/\beta$, that is $p(x,y,t)$ is approximately normal with expectation $F(x,y,t)$ and variance $\beta F(x,y,t)$. The approximation should be excellent since the expectation of the Poisson distribution, corresponding to pixel values, is at least 100 as estimated from our images.

The parameters β and F_0 can be estimated from the pre-bleach image(s) independent from the other model parameters. The expectation of a pixel value in the pre-bleach images is F_0 and its variance is βF_0. F_0 is estimated by the average pixel value in the pre-bleach image(s), while β is estimated by the variance of the pre-bleach pixel values divided by the estimate of F_0. The set of remaining model parameters $\theta = (D, k, K_0, r_{m,n}^2)$ are estimated by maximum likelihood. To indicate that $F(x,y,t)$ depends on the parameter vector θ we will write

$F(x,y,t;\theta)$ further on. The likelihood function for all pixels $(x,y)\in S$ for all times $t\in T$ can then be written as:

$$L(x,y,t;\theta)=\prod_{(x,y)\in S}\prod_{t\in T}\frac{1}{\sqrt{2\pi\beta F(x,y,t;\theta)}}\exp\left\{-\frac{\left(p(x,y,t)-F(x,y,t;\theta)\right)^2}{2\beta F(x,y,t;\theta)}\right\}. \quad (1.16)$$

The log-likelihood that is to be maximized, is given by:

$$\begin{aligned} l(\theta;x,y,t)=&-\frac{|S||T|}{2}\log 2\pi\beta-\frac{1}{2}\sum_{(x,y)\in S}\sum_{t\in T}\log F(x,y,t;\theta)\\ &-\frac{1}{2\beta}\sum_{(x,y)\in S}\sum_{t\in T}\frac{\left(p(x,y,t)-F(x,y,t;\theta)\right)^2}{F(x,y,t;\theta)}, \end{aligned} \quad (1.17)$$

where $|S|$ and $|T|$ denote the number of elements in the sets S and T. Let $\hat{\theta}$ denote the θ-value maximizing the log-likelihood. From the large sample theory for likelihood estimators it is known that $\hat{\theta}$ is asymptotically normal with a covariance matrix V_θ which is the inverse of the observed Fisher information, $I(\hat{\theta})$ whose (i,j)th element is given by:

$$-\frac{\partial^2}{\partial\theta_i\partial\theta_j}l(\theta)\bigg|_{\theta=\hat{\theta}}. \quad (1.18)$$

Hence the standard error of θ_i is given by the square root of the ith diagonal term of $I(\hat{\theta})^{-1}$.

When analyzing the rFRAP data by least squares fitting, we minimize:

$$Q(\theta)=\sum_{(x,y)\in S}\sum_{t\in T}p\left((x,y,t)-F(x,y,t;\theta)\right)^2. \quad (1.19)$$

While analysis based on standard least squares fitting is fast, the maximum likelihood method has the advantage of also giving standard errors for the estimated parameters. Note that, at the expense of additional programming and considerably extended computing time standard errors may also be obtained for the least squares fitting by use of bootstrap techniques [30].

3. Materials and methods

3.1 Confocal microscopy

Validation experiments were performed on a confocal laser scanning microscope (model MRC1024 UV, Bio-Rad, Hemel Hempstead, UK). A 488 nm line of a 4 W Ar-ion laser (model Stabilite 2017, Spectra-Physics, Darmstadt, Germany) was used for (single photon) imaging and photobleaching in combination with a 10× NA0.45 objective lens (CFI Plan Apochromat, Nikon, Badhoevedorp, The Netherlands). On the Bio-Rad MRC1024 UV, this lens achieves an imaging resolution of $r_{d,0}$ = 1.0 µm, as determined from images of 200 nm fluorescent nanospheres immobilized on a microscope slide.

The experiments on biopolymer mixtures were performed on a confocal laser scanning microscope (model TCP SP2, Leica, Heidelberg, Germany), equipped with a Linkam TMS 92 heating and cooling stage. The light source for imaging and bleaching was the 488 nm line from a built-in Ar-ion laser. An 63× NA0.90 HC PL APO water immersion objective lens was used. As the beam expander function was not used, the effective numerical aperture was lower than 0.90.

3.2 Test solutions

The validation measurements of the rFRAP method are performed on 150 kDalton FITC-dextran (Sigma-Aldrich, Bornem, Belgium) solutions prepared in HEPES buffer at pH 7.4. The concentration range in which a linear relation exists between the observed fluorescence and the concentration of the fluorophore was determined to be below 4 mg/ml. It was decided to use a 3 mg/ml FITC-dextran stock solution for all validation experiments.

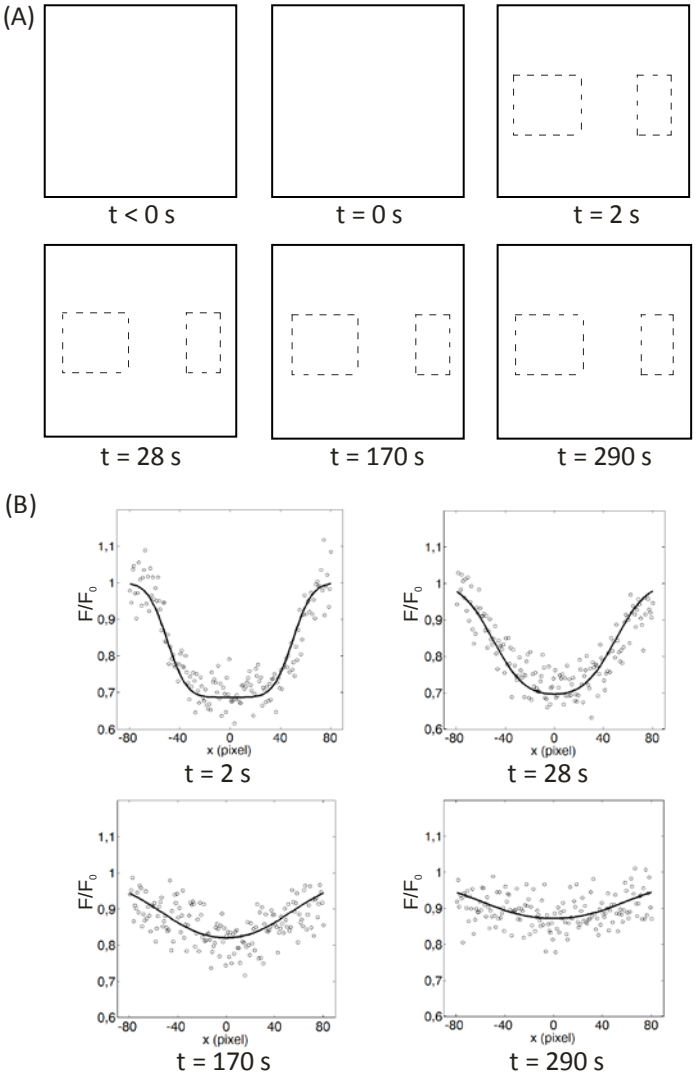

Fig. 2 : Illustration of an rFRAP experiment on a 150 kD FITC-dextran solution in HEPES buffer with 60% sucrose. (A) Several frames (512 by 512 pixels) of the time lapse movie are shown. The first frame shows the pre-bleach image. At time t=0 s, a square region is bleached (30 by 30 µm) at the left side of the field of view, as is illustrated in the second frame. The following frames show the fluorescence recovery at four different times after bleaching. The dashed square around the bleached area indicates the region that was taken into account in the analysis. The dashed rectangle to the right shows the region that was used for the background correction. (B) The intensity values with the result from the fitting procedure (solid line) are shown for a cross section along the x-direction of the square.

The solutions contained different amounts of sucrose in order to vary the dynamic viscosity η and to obtain diffusion coefficients in the range of 0.1 $\mu m^2/s$ to 10 $\mu m^2/s$. For rFRAP experiments, 5 µl of the FITC-dextran solution was dispensed on a microscope slide and sealed with a coverslip using a 120 µm thick double adhesive spacer (Secure-Seal Spacer, Molecular Probes, Leiden, The Netherlands).

3.3 Biopolymer mixtures

Biopolymer mixtures were prepared from gelatin LH type with Bloom 240 (System Bio Industries, Baupte, France) and Paselli SA2 maltodextrin (Avebe Group, Foxhol, Netherlands). The maltodextrin was covalently labeled with Rhodamine B isothiocyanate (RITC) to visually differentiate between gelatin and maltodextrin on the microscope images. Gelatin and RITC-maltodextrin were dissolved in a 150 ppm 10kDa FITC dextran solution under continuous slow agitation at 70 °C for 40 minutes and at 95 °C for 30 minutes, respectively. The gelatin and maltodextrin mixtures were subsequently mixed so that a final biopolymer concentrations of 4% w/w gelatin and 6% w/w maltodextrin was obtained. The mixture was put in a water bath at 70 °C to avoid a loss of heat and was stirred for a few minutes. The sample was subsequently transferred to a sample cup that was preheated to 70 °C in a furnace. The furnace was finally set to cool the sample from 70 °C to room temperature at 21 °C at a cooling rate of approximately 0.2 °C/min.

3.4 Measurement protocol

The validation experiments on the FITC-dextran solutions were performed in the middle of the sample, at approximately 60 µm above the coverslip. A typical FRAP measurement consisted of a time series of 30 images of 512 by 512 pixels, as illustrated in Fig. 2A. The first image shows the sample before bleaching, the second one shows the bleaching pattern at the time of bleaching, and the subsequent images show the recovery process after bleaching. The pattern is usually bleached at the left side of the image as this allows the user to define a background region at the right side of the image that is not affected by the diffusion front during the image acquisition. This background is used to correct for possible laser intensity fluctuations and bleaching during imaging.

The FRAP protocol for the experiments performed in biopolymer mixtures was as follows. First, 20 pre-bleach images were recorded after which a rectangle was photobleached in a single step. The AOTF was set to 100% to obtain maximal bleaching. In addition, the zoom-in-function was used to further increase the efficiency of the bleaching. Finally, 50 recovery images were recorded with an AOTF setting of 2%. The image format used, was 256 by 256 pixels with a scan rate of 800 Hz, leading to an image acquisition time of 0.5 s per image. The size of the bleaching region was between 5 by 5 µm and 10 by 10 µm. The sample was always examined in three dimensions before bleaching in order to avoid influence of the opposite phase along the z-direction.

3.5 Data analysis

Before fitting of the data to the rFRAP model, the recovery data was normalized to the fluorescence before bleaching, and corrected for intensity fluctuations and photobleaching during imaging. Normalization to the pre-bleach intensity was performed by dividing every pixel in the recovery images by the corresponding pixel in the pre-bleach image. To limit the corresponding amplification of noise, the pre-bleach image was first smoothed by a 15 by 15 pixel median kernel. Correction for laser fluctuations and bleaching during imaging is performed by dividing the pixels of each recovery images by the average value from a reference background region in the same image. As indicated in Fig. 2A, this reference region should be placed sufficiently far from the bleach region so as to remain unaffected by the diffusion front. Finally, the pixel values of the entire stack of images of the time lapse movie are simultaneously fitted (least squares fit or maximum likelihood analysis) to Eq. (1.13) and

(1.15) of the rFRAP model with custom written routines in Matlab (The Matworks, Natick, MA, USA). As motivated in section 2.2, Eq. (1.13) is used because in this work we have made use of a low NA lens for single-photon FRAP experiments. A representative example is shown in Fig. 2B. Details on the maximum likelihood estimation are discussed in the theory section. To limit the computation time, the analysis is performed on a subregion as illustrated in Fig. 2A usually consisting of the bleached area extended with 30 pixels in each direction. In our experience, including more pixels did not substantially improve the analysis precision.

4. Results

4.1 Validation of the rFRAP method

To validate the new rFRAP method, experiments are performed on 150 kD FITC-dextran (FD150) solutions in HEPES buffer. Different amounts of sucrose were added to obtain a wide range of viscosities and hence diffusion coefficients. The influence of several model parameters was assessed on the calculated diffusion coefficient, as is discussed in the sections below. In all cases, the free fitting parameters were the diffusion coefficient D, the bleaching parameter K_0, the mobile fraction k and the average squared resolution r^2. The mobile fraction was correctly found to be close to 1 throughout all the validation experiments independent of the other parameters and is therefore not discussed any further.

4.1.1 Time step

The first question that was addressed is if there is an influence of the frame rate on an rFRAP experiment. It is useful to consider this question in relation to a characteristic recovery time τ, which is defined as the average time it takes for a molecule with diffusion coefficient D to diffuse from the centre to the edge of the bleached region. In two dimensions this average time is given by:

$$\tau = \frac{(L/2)^2}{4D}, \qquad (2.1)$$

where L is the length of the shortest side of the rectangle. rFRAP measurements were performed on an FD150 solution (containing 24% sucrose) for different times Δt between the subsequent recovery images ($\Delta t = \tau$, $\Delta t = \tau/2$, $\Delta t = \tau/3$, $\Delta t = \tau/4$, $\Delta t = \tau/5$) using a constant square bleach region of 50 by 50 µm. Uniform disk FRAP measurements were performed on the same sample to obtain an independent reference value for the diffusion coefficient [17]. In Fig. 3A the diffusion coefficient as obtained from the rFRAP experiments (n=5, with n the number of performed rFRAP experiments) is plotted as a function of the time step Δt, from which it is clear that the calculated diffusion coefficient is hardly influenced by the selected frame rate. The data suggest a slight increase (~5%) of the measured diffusion coefficient for smaller time steps. However, this could very well be due to some polydispersity of the FITC-dextrans because of which the larger and more slowly moving molecules are contributing less to the recovery at short time intervals. From this result it was decided to use a time interval $\Delta t = \tau$ for all further experiments.

Eq. (2.1) is also useful to make sure that the acquisition time of a single image is small compared to the typical recovery time so that the image can be considered as a snapshot of the fluorophore concentration distribution at that time. In case of very slow scanning rates, the pixels at the beginning of the image would be recorded at a substantially different time than the last pixels in the same image, which could lead to erroneous results.

4.1.2 Diffusion during bleaching

In the theoretical derivation of the rectangle FRAP model we assumed that bleaching happens instantaneous so as to ignore diffusion during bleaching. However, on a laser scanning

microscope the bleaching can never be entirely instantaneous. This is because of the scanning motion of the laser beam by which the last pixels of the bleach area are bleached at a later point in time than the first ones. The experimental bleach step therefore deviates from the theory by the fact that the rectangle (or any other shape) is not bleached at once and that diffusion inside the bleach area might already start during the bleaching step. This can result in a deviation of the effective initial profile of the bleached fluorophores from the theoretically expected one [10,31]. Therefore, we have explicitly tested the effect of diffusion during photobleaching on the measured diffusion coefficient for a number of bleach times. The experiment was carried out on an FD150 solution (16% sucrose) in which square regions of 20 µm × 20 µm were bleached with different zoom settings so as to obtain different bleaching times. The amount of photobleaching was kept below 50% for all zoom settings, this will be shown to be valid in section 4.1.3.

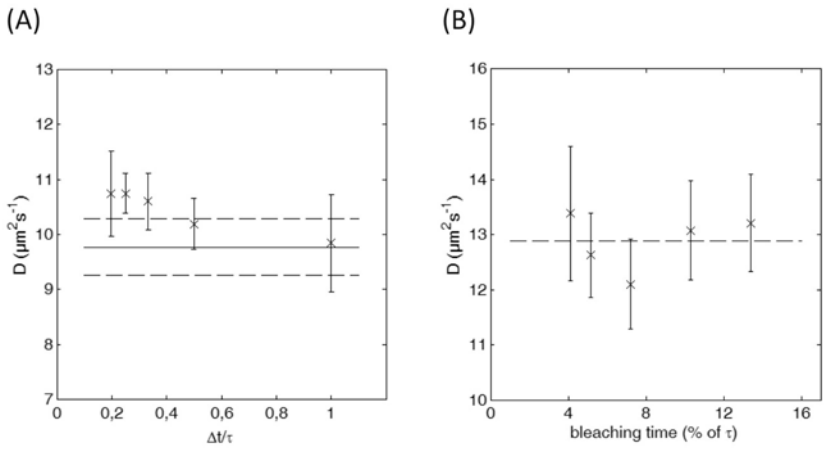

Fig. 3 : (A) The average diffusion coefficient of 5 rFRAP measurements on a FD150 solution (24% sucrose) is plotted as a function of the time interval Δt (relative to the characteristic recovery time τ) between the images. In all cases a square region of 50 by 50 µm was bleached. The solid horizontal line indicates the diffusion coefficient of a uniform disk FRAP reference measurement (D=9.8±0.5 µm^2/s). The dashed lines indicate the corresponding standard deviation of 0.5 µm^2/s. (B) The average diffusion coefficient for rFRAP measurements on FD150 solutions with 16% sucrose in function of the bleaching time (expressed as the percentage of the characteristic recovery time τ) that was needed in order to bleach a square of 20 by 20 µm. The dashed line indicates the average value of the data points (D=12.88±1.0 µm^2/s).

The results are shown in Fig. 3B (n=10) where the measured diffusion coefficient is plotted versus the bleaching time which is expressed as a percentage of the recovery time τ (see Eq. (2.1)). Within the tested range of 4-14% (which was maximum for our CLSM), no significant difference could be found in the measured diffusion coefficient. This demonstrates the capability of the rectangle FRAP method to compensate for at least a limited amount of diffusion during bleaching. All further experiments reported here were conducted with bleaching times shorter than 14% of the recovery time τ.

4.1.3 Amount of photobleaching

An important assumption in the rFRAP model is the linearity of the photobleaching process (cfr. Eq. (1.6)). Since normally the photobleaching process is modeled as an exponential decay, in theory this could mean that only a small amount of bleaching is allowed (<30%). We tested this experimentally on a FD150 solution (52% sucrose) for different percentages of photobleaching of a 5 by 5 µm square bleach region. The percentage of photobleaching was

calculated using Eq. (1.14). The amount of photobleaching was increased by increasing the zoom setting of the microscope.

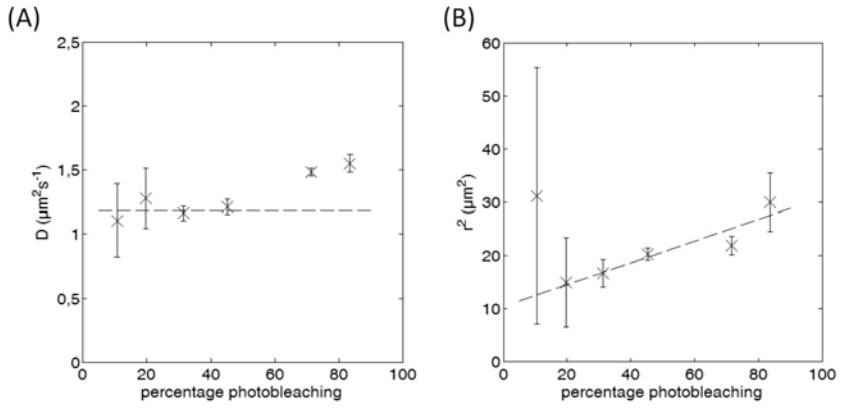

Fig. 4 : rFRAP measurements for different bleaching percentages on an FITC-dextran solution. (A) The average diffusion coefficient is plotted in function of percentage of bleaching. The straight dashed line represents the average value over the first 3 data points. (B) The resolution parameter is shown in function of the percentage of bleaching. The dashed line represents a linear fit to the measured average values (the data point at 10% was excluded).

As indicated in Fig. 4A (n=5), the diffusion coefficient was found to be constant within the experimental precision for at least up to ~50% of photobleaching. Apparently the (possible) deviation from linearity is counter-acted by an increase of the resolution parameter r^2 (see Fig. 4B). However, when increasing the amount of photobleaching further to 70-90%, the resolution parameter cannot fully compensate for the deviation from linearity leading to a modest over-estimation (~25%) of the diffusion coefficient. We conclude that the calculated diffusion coefficient by the rFRAP method in practice is independent of the amount of photobleaching for at least up to 50%.

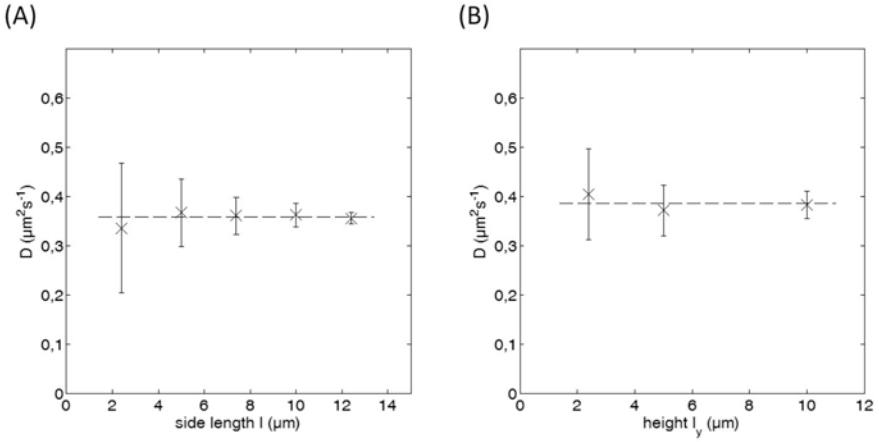

Fig. 5 : (A) The average diffusion coefficient for rFRAP measurements on FITC-dextran solutions with 60% sucrose in function of the size of the bleached square with side length l. The dashed line indicates the average value of the data points. (B) The diffusion coefficient is calculated from rFRAP measurements on an FD150 solution (60% sucrose) using rectangles of length 10 μm but with a varying height l_y. The dashed line indicates the average value over all measurements.

4.1.4 Rectangle size

Since in the derivation of the rFRAP model we have included the effective photobleaching resolution as well as the imaging resolution, the method should be valid for all sizes of the bleaching rectangle. This was tested on an FD150 solution (60% sucrose) by photobleaching square regions of different sizes: 2.4 µm, 5 µm, 7.4 µm, 10 µm and 12.4 µm. The results are shown in Fig. 5A (n=10), from which it is clear that the calculated diffusion coefficient is indeed independent of the size of the bleach region. The standard error on the average D values increases for smaller sizes of the bleach region since the available number of pixels in the data set decreases.

4.1.5 Rectangle aspect ratio

In a next step we tested the validity of the rectangle FRAP method for different aspect ratios of the rectangle. rFRAP experiments were performed on an FD150 solution (60% sucrose) for bleach rectangles all having a width of 10 µm, but a variable height: 2.4 µm, 5 µm and 10 µm. The results in Fig. 5B (n=5) confirm that the diffusion coefficient is independent of the aspect ratio. The larger the height of the rectangle, the more precise the diffusion coefficient could be determined because of more pixels being available in the bleached area.

4.1.6 Validation of the calculated diffusion coefficient

The diffusion coefficients predicted by the new rFRAP model are validated against measurements by the uniform disk model on FD150 solutions containing different amounts of sucrose : 0%, 5%, 10%, 16%, 24%, 32% and 44%. The uniform disk model is used as a reference since it is an independent FRAP method that has been extensively validated [17].

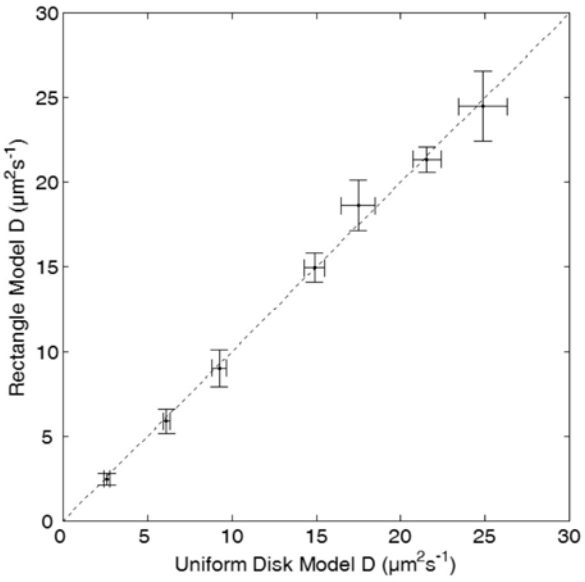

Fig. 6 : The average diffusion coefficient D as determined by the rFRAP method is plotted vs. the average diffusion coefficient D determined by the disk model for FD150 solutions with different amounts of sucrose. The dashed line represents the ideal case in which both methods predict exactly the same diffusion coefficient.

For all measurements a rectangle of 30 by 30 µm and a disk of 50 µm diameter was used. Smaller regions could not be used for comparison because, as opposed to the rFRAP model, the uniform disk model requires large bleach areas since it does not take the effective

bleaching resolution into account. The effect of the size of the bleaching region on the estimated diffusion coefficient was discussed separately in section 4.1.4. As can be seen from the data in Fig. 6, the rFRAP measurements are in excellent agreement with the disk FRAP measurements. A linear fit to the data yields a slope of 1.0065 and an offset of -0.0987 $\mu m^2/s$. An additional two-tailed *t*-test confirmed that the rFRAP measurements are not different from the disk FRAP measurements at the 5% significance level. Despite the extra free fitting parameter in case of the rectangle method (average squared resolution r^2), the precision of the individual diffusion coefficients is similar for both methods, ranging between between 5% and 15%. This can be attributed to the spatial information that is taken into account by the rFRAP method. We conclude that the rFRAP method is capable of accurately measuring diffusion for a wide range of diffusion coefficients with good precision.

4.1.7 Comparison of least squares estimation and maximum likelihood estimation

Maximum Likelihood (ML) was recently suggested as an alternative to the classic least-squares (LS) fit for analysis of FRAP data [21], because this framework allows for estimation of standard errors for parameter estimates and more generally estimation of variance components for more complicated experimental designs. It is therefore interesting to compare both analysis methods side by side. A series of rFRAP experiments was performed on an FD150 solution (60% sucrose) using a constant bleach region but an increasing laser intensity so as to obtain a range of different K_0 and r^2 values. These data sets were analyzed by both LS and ML.

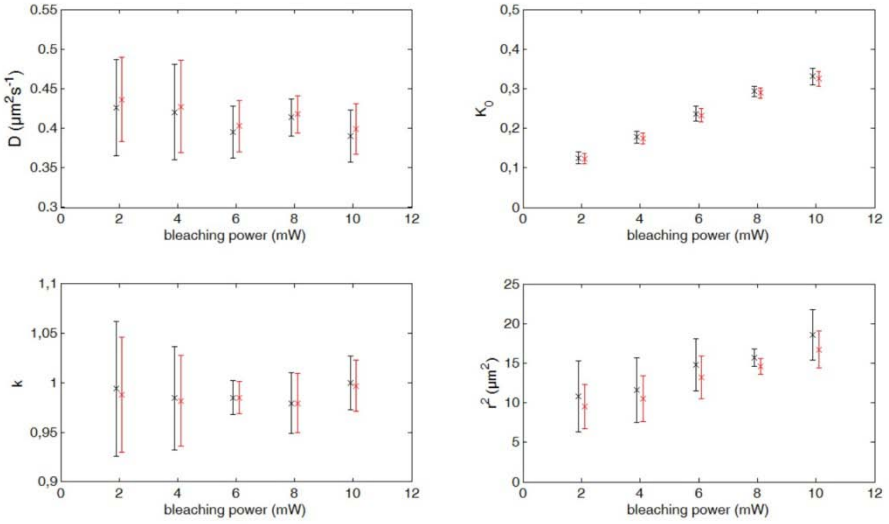

Fig. 7 : Comparison of least squares estimates (black) and maximum likelihood estimates (red) for rFRAP experiments performed on an FD150 solution (60% sucrose) using a constant bleach region but an increasing laser intensity between 2 mW and 10 mW. Averages of 10 measurements are shown with error bars corresponding to one standard deviation.

As can be seen in Fig. 7, the estimates of *D*, *k* and K_0 are essentially the same for both analysis methods, whereas r^2 is slightly lower for the ML estimation. The standard deviations of the estimates are also similar but generally a little smaller for the ML method. The computation time for the ML method was generally longer than for the LS method, particularly if the initial guesses of the unknown parameters were far from the optimal values. The main advantage of the likelihood method is that it can easily produce standard errors for the estimated parameters. These can be used both to get an idea of the precision of the estimates and to give prediction bounds in residual plots as a guideline for the quality of the

model fit. This is especially useful in case of heterogeneous samples where it might be difficult to repeat FRAP experiments under identical conditions and thus to obtain the standard error from repeated measurements. We note that in some cases it was difficult to come to a good estimate of the resolution parameter r^2 by direct optimization of the likelihood. In this case, iteration with the profile likelihood [29] turned out to be useful.

4.2 rFRAP measurements on biopolymer mixtures

Mixed biopolymer systems are widely utilized in industries for foods, pharmaceuticals and personal care to control texture and mass transport in a product. Many mixed biopolymer systems are incompatible and will phase separate and gel under certain conditions. The protein-polysaccharide mixture of gelatin and maltodextrin is a thermodynamically instable system, having a segregative phase separation process generating regions enriched in either one of the polymers [32,33]. In addition, the system will gel when a temperature below the gelling temperature of gelatin is reached, which kinetically traps the system in a nonequilibrium state.

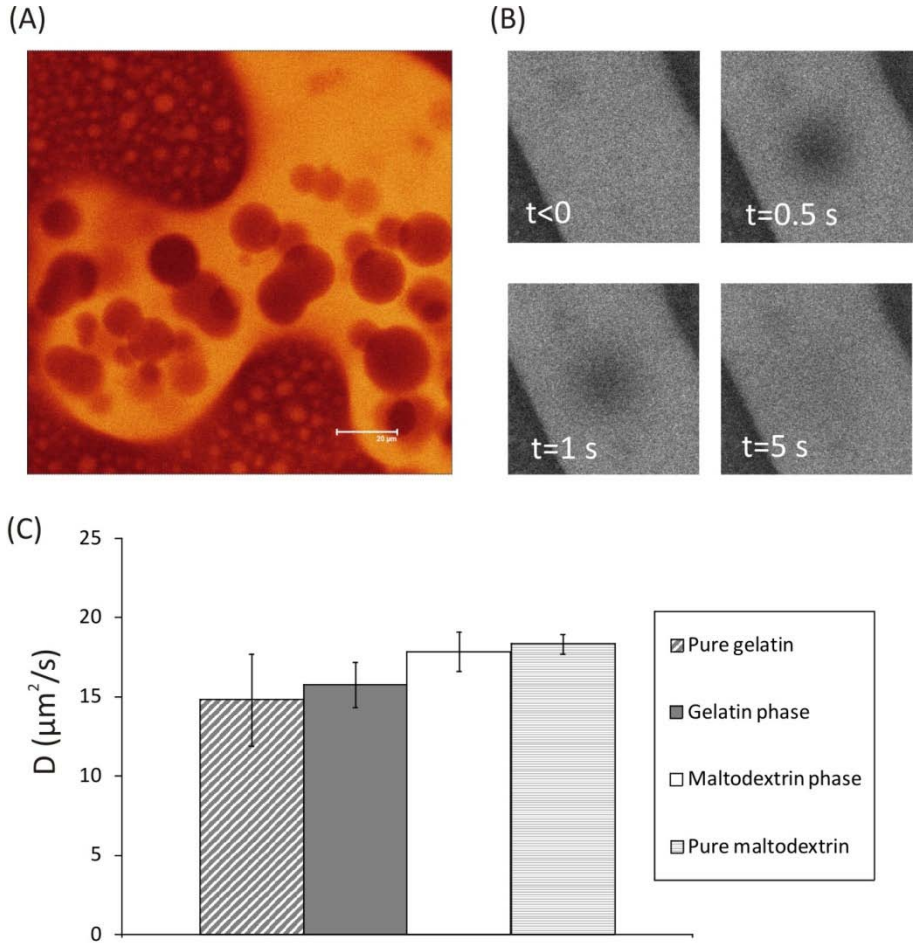

Fig. 8 : (A) CLSM image of a kinetically trapped and phase separated gelatin/maltodextrin mixture. The maltodextrin phase is bright and the gelatin phase is dark. The scale bar is 20 μm. (B) An rFRAP measurement in the maltodextrin phase of a phase separated gelatin/maltodextrin system. The bleached square is 7 by 7 μm and the field of view is 60 by 60 μm. (C) Diffusion coefficients determined using rFRAP in pure gelatine and maltodextrin, as well as in the pase-separated gelatin/maltodextrin mixture.

The final morphology of the mixed biopolymer system will be determined by the kinetics of phase separation and gelation together with the relative rate between the two processes [34]. By changing the biopolymer concentration, quench temperature, cooling rate, ionic conditions and confinement, it has been shown that the morphology of the gelatin-maltodextrin system can be designed to desired microstructures [35].

Kinetically trapped phase separated biopolymer mixtures, such as mixtures of gelatin and maltodextrin, often have a very heterogeneous microstructure. Fig. 8A shows an example of such a structure with 4 w/w% gelatin and 6 w/w% maltodextrin. The dark phase is the gelatin phase and the bright phase is the maltodextrin phase. It can be seen that the structure is very heterogeneous with a bicontinuous morphology that contains spherical inclusions of the opposite phase. The characteristic length scales of the phase separated domains in this system ranges from a few micrometers up to hundreds of micrometers. One of the main objectives with the rFRAP method is to measure the local diffusion rate in small regions of such heterogeneous materials.

Fig. 8B shows an rFRAP experiment in the maltodextrin phase of a kinetically trapped and phase separated gelatin/maltodextrin mixture containing FITC-dextran molecules of 10 kDalton. The first (t<0) and second (t=0.5 s) image in Fig. 8B shows the structure before bleaching and after bleaching, respectively. Images 3 (t=1 s) and 4 (t=5 s) show the subsequent fluorescence recovery of the FITC-dextran molecules.

Fig. 8C shows the results from rectangle FRAP measurements in both the pure gelatin and maltodextrin gels, as well as in the gelatin and maltodextrin phases of the kinetically trapped phase separated mixture. The leftmost and the rightmost bar in Fig. 8C are the diffusion rates in pure gelatin and pure maltodextrin respectively. The diffusion coefficient of FITC-dextran 10 kDa in pure gelatin is 14.8 ± 2.9 $\mu m^2/s$ and 18.3 ± 0.6 $\mu m^2/s$ in pure maltodextrin. The diffusion coefficient obtained by rFRAP in the phase-separated mixture is 15.8 ± 1.4 $\mu m^2/s$ (n=14) in the gelatin phase and 17.9 ± 1.2 $\mu m^2/s$ in the maltodextrin phase (n=13). The diffusion coefficients in the phase separated system differ slightly from the values obtained in corresponding pure phases. This can be attributed to the fact that the maltodextrin phase will always contain a small amount of gelatin and vice versa due to entropic reasons. This means that the gelatin will contribute to the diffusion rate in maltodextrin and maltodextrin will contribute to the diffusion in gelatin. A t-test performed on the data from the polymer mixture showed that the diffusion coefficients in the different phases was significantly different with a p-value of 0.0004. It can therefore be concluded that rFRAP has the power to differentiate between the diffusion rate of FITC-dextran in the individual phases in a heterogeneous phase separated and gelled biopolymer mixture even when the difference is small.

5. Discussion

Over the years, FRAP has become one of the most well-known methods to study local diffusion on the micrometer scale in biological media and biopharmaceutical materials. While several quantitative FRAP methods have been put forward in literature, it is a fact that most of the reported applied FRAP mobility studies remain qualitative or semi-quantitative at best because of the limited usefulness or complexity of published FRAP methods. In order to bring quantitative FRAP measurements to the larger community of biologists and material scientists, we feel there is a clear need for FRAP methods that are more versatile, are easily implemented on commercial microscopes and allow for straightforward and fast data analysis. Here we have addressed this need by developing a new pixelbased FRAP method with a closed-form expression that describes the full temporal and spatial information of the recovery process. A closed-form expression could be obtained by assuming a rectangular bleaching area and making the assumption of a linear photobleaching process. Note that a similar closed-formed expression is currently not available for the conventionally used circular bleaching area. By taking into account the relevant microscope resolution parameters (effective photobleaching resolution and imaging resolution), the rectangle can have any size

and aspect ratio, even down to the size of the point spread function. We have shown before that the effective photobleaching resolution can be substantially larger than the theoretical one because of triplet saturation of the fluorophores that might arise during the highly intense photobleaching phase [14,15]. The actual value of the effective photobleaching resolution depends on the excitation photon flux, the photochemical properties of the fluorophore and the local chemical environment. Hence it is important to include the photobleaching and imaging resolution as independent parameters. Nevertheless, in the final expression of the rFRAP model, both resolution parameters combine to a single one (the average square resolution r^2) that can be included as a free fitting parameter during the data analysis, thus eliminating the need for prior calibration. Including r^2 as a free fitting parameter is possible since not only temporal but also spatial information is taken into account.

Using well-characterized FITC-dextran solutions we have shown that the rFRAP method can reliably measure the diffusion coefficient in a wide range of conditions. It was demonstrated that the rectangle can be arbitrarily small or large with any aspect ratio. Furthermore it was shown that, despite the theoretical assumption of linear photobleaching, substantial photobleaching up to at least 50% is allowed thanks to including the resolution r^2 as a free fitting parameter, which was found to increase with increasing bleaching power, as expected [14,15]. Diffusion during bleaching was found to have a negligible effect on the predicted diffusion coefficient. This can be explained by the fact that the rectangle FRAP model is based on a rectangular bleach area that is convolved with a Gaussian function (cfr. Eq. (1.2)). Although the original reason was to incorporate an independent effective bleaching intensity distribution, it is not surprising that diffusion during bleaching can also be captured by this convolution since the progression of free diffusion follows from a Gaussian propagator as well (cfr. Eq. (1.7)). Finally, the rFRAP method was thoroughly validated against conventional large disk FRAP measurements on a series of FITC-dextran solutions with different viscosities.

In the data analysis of the rFRAP method, two fitting algorithms were evaluated, the least squares method and the maximum likelihood method. We found that the classic least squares fit gives acceptable results, while the maximum likelihood method can obtain slightly improved estimates at the expense of a longer calculation time. However, a major advantage of the maximum likelihood method is that standard errors can be easily calculated from a single experiment. This is an advantage in case of heterogeneous samples where it might be difficult to obtain repetitions of exactly the same measurement. As mentioned in Section 2.3, with additional programming and extended computing time standard errors may also be obtained for least squares fitting by use of bootstrap techniques.

The rFRAP method was finally used to study the diffusion coefficient in a phase separated mixture of gelatin and maltodextrin having characteristic length scales between five and hundreds of micrometers. Due to its ability to perform diffusion measurements in small regions, the diffusion coefficient in the separate phases could be accurately determined.

6. Conclusions

The rFRAP method proves to be a versatile approach for accurate and precise diffusion measurements by a (confocal) laser scanning microscope. Because the model can make use of a closed-form solution describing the full recovery in time and space, independent calibration of the effective microscope resolution parameters is no longer required. Combined with the possibility to photobleach rectangles of any size and aspect ratio, it opens up the field for performing diffusion measurements on both small and large samples with our without heterogeneous structures on the micrometer length scale.

Acknowledgements

Financial support by the Ghent University Special Research Fund and the Fund for Scientific Research Flanders (Belgium) is acknowledged with gratitude. Hendrik Deschout is a doctoral

fellow of the Institute for the Promotion of Innovation through Science and Technology in Flanders (IWT), Belgium. Niklas Lorén, Joel Hagman and Sophia Fransson gratefully acknowledge the financial support from VINNOVA through the VINN Excellence Centre SuMo Biomaterials (Supermolecular Biomaterials-Structure dynamics and properties). Jenny Jonasson and Mats Rudemo have been supported by the Swedish Foundation for Strategic Research through the Gothenburg Mathematical Modelling Center and the Swedish Research Council through the Gothenburg Stochastic Centre.